Supplemental Material for Simultaneous Excitation of Two Atoms with a Single Photon

I. DERIVATION OF THE EFFECTIVE HAMILTONIAN

According to standard time-dependent perturbation theory, for a constant perturbation switched-on at $t = 0$, the resulting transition rate can be expressed as

$$W_{i\to f} = \frac{2\pi}{\hbar}|V_{fi}^{\text{eff}}|^2\,\delta(E_f - E_i)\,, \tag{1}$$

where i and f label the initial and final states with corresponding energies E_i and E_f, and V_{fi}^{eff} describes the effective coupling strength connecting the initial and final states. In the framework of first-order perturbation theory, this effective coupling strength coincides with the matrix element of the generic perturbing interaction $\hat{V}$: $V_{fi}^{\text{eff}} = V_{fi} = \langle f|\hat{V}|i\rangle$. If i and f are coupled only via third-order perturbation theory, the resulting effective coupling strength is

$$V_{fi}^{\text{eff}} = \sum_{m,n} \frac{V_{fn}V_{nm}V_{mi}}{(E_i - E_m)(E_i - E_n)}\,. \tag{2}$$

In the case when the states $|n\rangle$ and $|m\rangle$ are virtual intermediate states that do not conserve energy, the only effect of the perturbation is to couple, via these virtual intermediate states, the initial and final states. The same coupling can be described by the effective Hamiltonian

$$H_{\text{eff}} = V_{fi}^{\text{eff}}\,|f\rangle\langle i| + \text{H.c.}\,, \tag{3}$$

with V_{fi}^{eff} provided by Eq. (2).

We observe that, applying first-order perturbation theory by using this effective Hamiltonian, we obtain the same result of standard third-order perturbation theory with the real perturbation $\hat{V}$. Hence, Eq. (2) describes the effective coupling strength between the energy-degenerate states $|g, g, 1\rangle$ and $|e, e, 0\rangle$. We consider the case $\omega_{\text{c}} \approx 2\omega_{\text{q}}$ and a perturbation of the form:

$$\hat{V} = \lambda\hat{X}\sum_i(\cos\theta\,\hat{\sigma}_x^{(i)} + \sin\theta\,\hat{\sigma}_z^{(i)})\,. \tag{4}$$

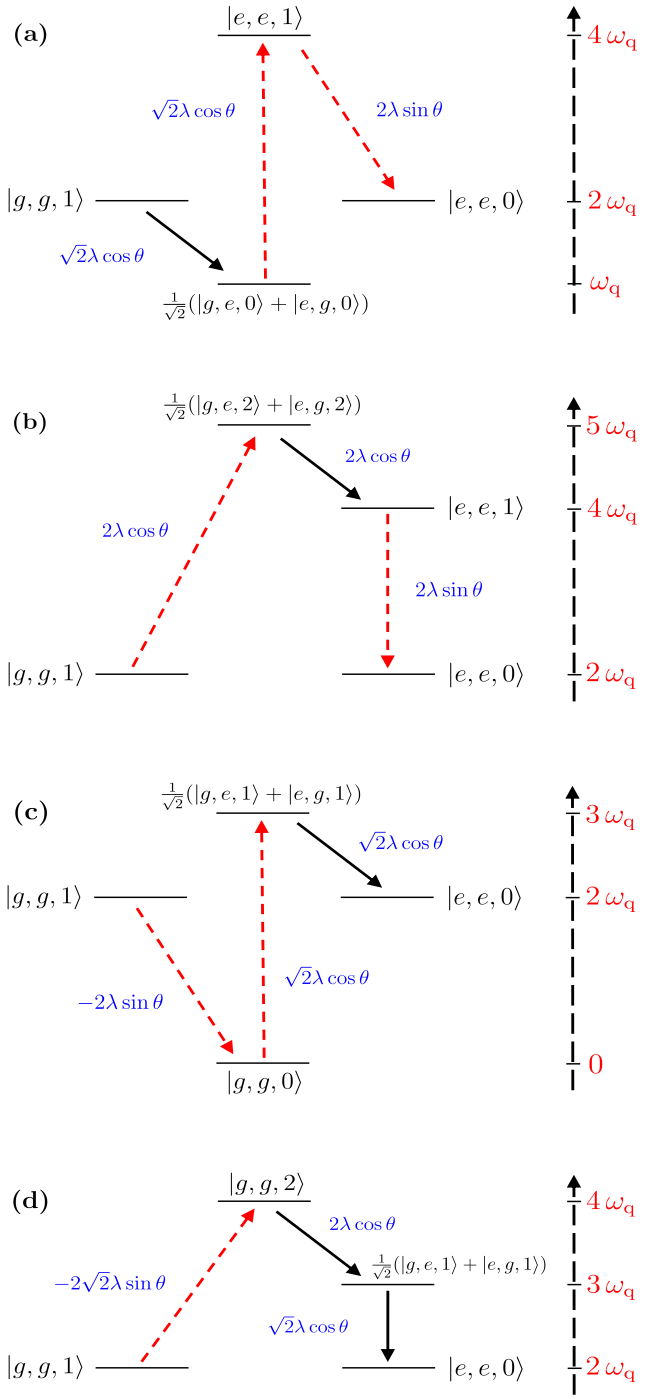

FIG. S1. (Color online) Coupling between the bare states $|g,g,1\rangle$ and $|e,e,0\rangle$ via intermediate virtual transitions. Here, the excitation-number nonconserving processes are represented by the arrowed red dashed lines. The transition matrix elements are also shown (in blue).

After carefully inspecting all the possible intermediate states, we find that only the four paths shown in Fig. S1 can connect the states $|g,g,1\rangle$ and $|e,e,0\rangle$. Applying Eq. (2), we obtain,

$$\Omega_{\rm eff} \equiv -V_{fi}^{\rm eff} = \frac{8}{3}\sin\theta\cos^2\theta\left(\frac{\lambda}{\omega_{\rm q}}\right)^3 . \tag{5}$$

Figure S2 displays the comparison of the magnitudes of the effective Rabi splitting $2\Omega_{\rm eff}/\omega_{\rm q}$ between the states $|g,g,1\rangle$ and $|e,e,0\rangle$ obtained analytically [Eq. (5)] via third-order perturbation theory and by the numerical diagonalization of the Hamiltonian in Eq. (1) (in the main text), as a function of the normalized interaction strength $\lambda/\omega_{\rm q}$. The agreement is very good, also for coupling strengths λ beyond 10% of the qubit transition frequency $\omega_{\rm q}$. This result confirms the $(\lambda/\omega_{\rm q})^3$ proportionality of the effective (one-photon)-(two-atoms) coupling predicted by the above analysis.

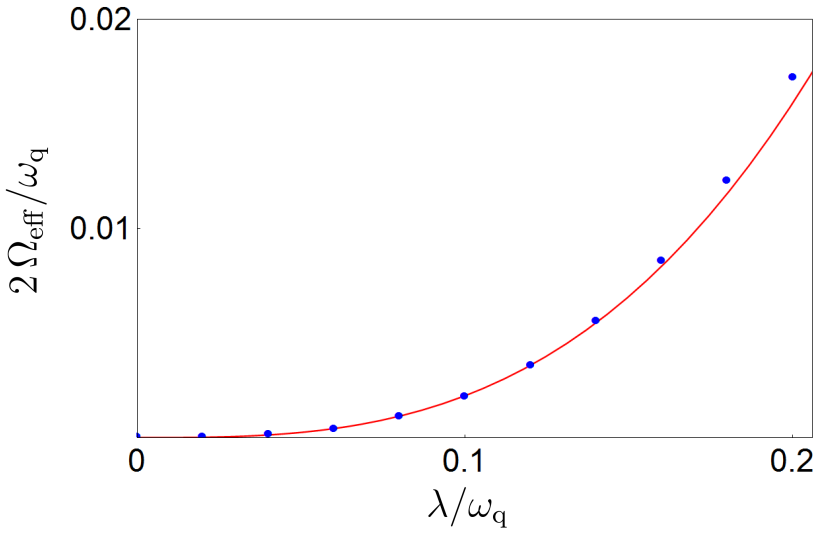

FIG. S2. (Color online) Comparison between the numerically-calculated normalized Rabi splitting (points) (corresponding to twice the effective coupling between one cavity photon and two independent atoms) and the corresponding calculation using third-order perturbation theory (continuous red curve).

II. A SINGLE PHOTON CAN SIMULTANEOUSLY EXCITE THREE QUBITS

If the resonance frequency of the optical/microwave resonator is $\omega_{\rm c} \approx 3\omega_{\rm q}$, the simultaneous excitation of three atoms: $|g,g,g,1\rangle \rightarrow |e,e,e,0\rangle$ is also possible. In contrast to

the two-atom process, the three-atom process does not need broken symmetry. This point can be understood considering one of the possible paths (involving three virtual transitions) which can determine the resonant coupling $|g,g,g,1\rangle \leftrightarrow |e,e,e,0\rangle$. In this case we consider the following perturbing potential,

$$\hat{V} = \lambda \sum_{i=1}^{3} (\hat{a}\sigma_{+}^{(i)} + \hat{a}^{\dagger}\sigma_{-}^{(i)} + \hat{a}\sigma_{-}^{(i)} + \hat{a}^{\dagger}\sigma_{+}^{(i)}) \,, \tag{6}$$

corresponding to the case $\theta = 0$, where parity symmetry is not broken. According to third order perturbation theory, one of the possible paths is: $|g,g,g,1\rangle \rightarrow |(e,g,g)_s,2\rangle \rightarrow |(e,e,g)_s,1\rangle \rightarrow |e,e,e,0\rangle$, where we indicated with $()_s$ the symmetric states of three qubits with one or two of them in the excited state. The first virtual transition $|g,g,g,1\rangle \rightarrow |(e,g,g)_s,2\rangle$ is induced by the counter rotating terms $\hat{a}^{\dagger}\sigma_{+}^{(i)}$ in Eq. (6), while the last two transitions are induced by the JC interaction terms $\hat{a}\sigma_{+}^{(i)}$.

Figure S3a displays the lowest energy states (specifically, we report the frequency differences $\omega_{i,0} = \omega_i - \omega_0$) as a function of the resonator frequency resulting from the numerical diagonalization of the total Hamiltonian including the resonator energy, the three qubits energy and the interaction energy in Eq. (6). We used $\lambda/\omega_{\rm q} = 0.3$ and $\theta = 0$. At $\omega_{\rm c} \simeq 2.86\,\omega_{\rm c}$ an apparent crossing can be observed. Actually, what appears as a crossing on this scale, it turns out to be a splitting anticrossing on an enlarged view as in Fig. S3b. The resulting states are well approximated by the states $(|e,e,e,0\rangle \pm |g,g,g,1\rangle)/\sqrt{2}$. This splitting is not present in the rotating-wave approximation (RWA), where the coherent coupling between states with a different number of excitations is not allowed. Figure S4 displays the numerically-calculated dynamics of the photon number $\langle \hat{X}^{-}\hat{X}^{+}\rangle$, of the mean excitation number $\langle \hat{C}_1^{-}\hat{C}_1^{+}\rangle$ for one of the qubits (which, of course, coincides with that of the other two), and of the three-qubit correlation $G_{\rm q}^{(3)} = \langle \hat{C}_1^{-}\hat{C}_2^{-}\hat{C}_3^{-}\hat{C}_3^{+}\hat{C}_2^{+}\hat{C}_1^{+}\rangle$. Vacuum Rabi oscillations showing the reversible excitation exchange between the three qubits and the resonator are clearly visible. We also observe a strong three-qubit correlation, since $\langle \hat{C}_1^{-}\hat{C}_1^{+}\rangle$ and $G_{\rm q}^{(3)}(t)$ are almost coincident. This is a clear signature that the three qubits are jointly excited. Moreover, we observe that $\langle \hat{X}^{-}\hat{X}^{+}\rangle$ is not zero at the photon minima. This occurs because, owing to the same processes inducing its coupling with the one-photon state, the three-qubit excited state —eee0¿ acquires a non-negligible dipole transition matrix element, so that it is able to emit photons after decaying into the lower energy states (see Fig S3a).

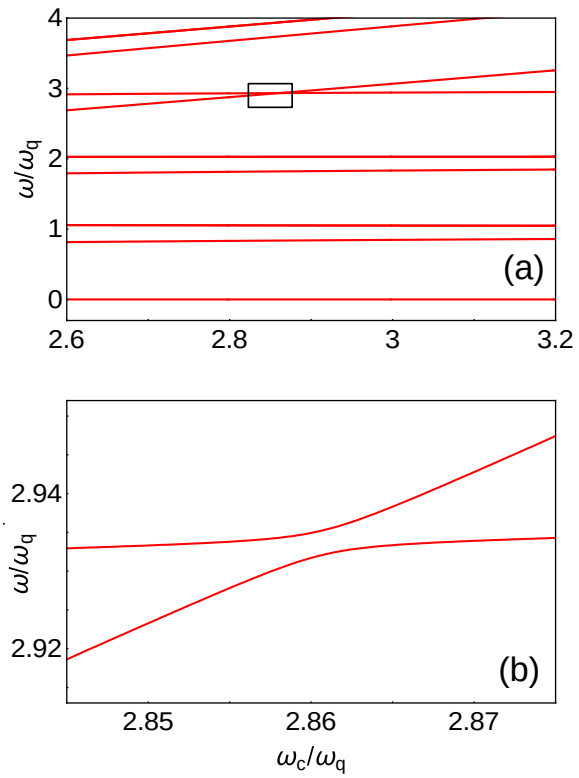

FIG. S3. (Color online) (a) Energy levels as a function of $\omega_{\rm c}/\omega_{\rm q}$ for the system of three qubits interacting with a resonator. Here we consider a normalized coupling rate $\lambda/\omega_{\rm q} = 0.1$ between the resonator and each of the qubits. We used $\theta = 0$ and $\lambda/\omega_{\rm q} = 0.3$. (b) Enlarged view of the spectral region delimited by a square in panel (a). This shows an avoided-level crossing, demonstrating the coupling between the states $|g, g, g, 1\rangle$ and $|e, e, e, 0\rangle$ due to the presence of counter-rotating terms in the system Hamiltonian.

III. ADDITIONAL ATOMIC TRANSITIONS

We discuss here the case of two identical atoms coupled to a single resonator-mode beyond the two-level system description. We consider the case where each of them has an additional higher energy state $|f\rangle$. We also assume that the transition $|g\rangle \leftrightarrow |f\rangle$, with frequency ω_{fg} is optically active. By using the results of the Supplementary Sect. I, the effective system Hamiltonian can be written as,

$$\begin{aligned}\hat{H}_{\rm eff} &= \omega_{\rm c}|g,g,1\rangle\langle g,g,1| + 2\omega_{eg}|e,e,0\rangle\langle e,e,0| + \omega_{fg}|(f,g)_s,0\rangle\langle(f,g)_s,0| \\ &+ \Omega_{\rm eff}(|g,g,1\rangle\langle e,e,0| + {\rm H.c.}) + \lambda'(|g,g,1\rangle\langle(f,g)_s,0|\,, \end{aligned} \tag{7}$$

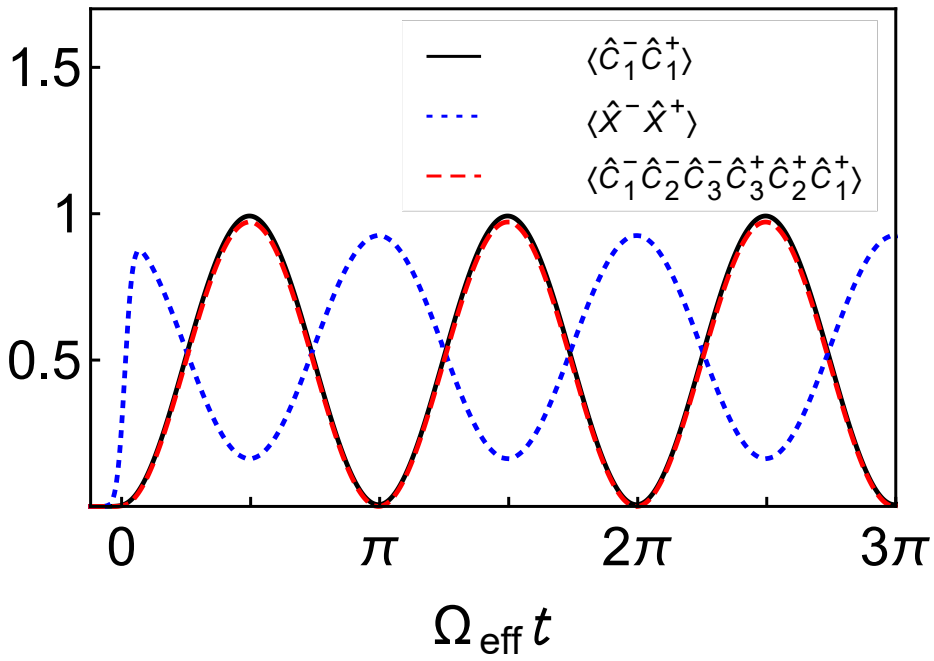

FIG. S4. (Color online) Time evolution of the cavity mean photon number $\langle \hat{X}^- \hat{X}^+ \rangle$ (dotted blue curve), qubit 1 mean excitation number $\langle \hat{C}_1^- \hat{C}_1^+ \rangle$ (continuous black curve), and the zero-delay three-qubit correlation function $G_{\rm q}^{(3)} = \langle \hat{C}_1^- \hat{C}_2^- \hat{C}_3^- \hat{C}_3^+ \hat{C}_2^+ \hat{C}_1^+ \rangle$ (dashed red curve) after the arrival of a π-like Gaussian pulse initially exciting the resonator. After the arrival of the pulse, the system undergoes vacuum Rabi oscillations showing the reversible joint absorption and re-emission of one photon by three qubits. $\langle \hat{C}_1^- \hat{C}_1^+ \rangle$ and $G_{\rm q}^{(3)}(t)$ are almost coincident.

where $|(f,g)_s,0\rangle = (|f,g,0\rangle + |g,f,0\rangle)/\sqrt{2}$, describes a symmetric superposition where only one of the two atoms is in the excited state $|f\rangle$, and λ' is the coupling rate between the cavity photon and the transition $|g\rangle \leftrightarrow |f\rangle$.

We consider the case $\omega_{\rm c} = 2\omega_{\rm eg}$. Starting from the atoms in the ground state and a single photon in the resonator: $|\psi(0)\rangle = |g,g,1\rangle$, the system will evolve towards the following superposition,

$$|\psi(t)\rangle = a(t)|g,g,1\rangle + b(t)|e,e,0\rangle + c(t)|(f,g)_s,0\rangle\,, \tag{8}$$

where the excitation of largely detuned states, as $|(f,e)_s,0\rangle$ and $|f,f\rangle$, has been neglected. We study the system dynamics for different detunings $\Delta = \omega_{fg} - \omega_{\rm c} = \omega_{fe} - \omega_{eg}$. The normalized detuning Δ/ω_{eg} also provides a measure of the atomic anharmonicity. In addition to the simultaneous excitation of two atoms (described by the ket $|e,e,0\rangle$), the excitation of

only one of them, described by the ket $|(f,g)_s,0\rangle$ in Eq. (8) is also possible. The probability that atom 1 is in an excited state can be derived from the mean value of the operator $\hat{P}_1^{\rm exc} = |e\rangle\langle e| + |f\rangle\langle f|$, where the bras and the kes here referes to states of the atom 1. The probability that both atoms are in an excited state can be expressed as the mean value of the operator $\hat{P}_{12}^{\rm exc} = |e,e\rangle\langle e,e|$.

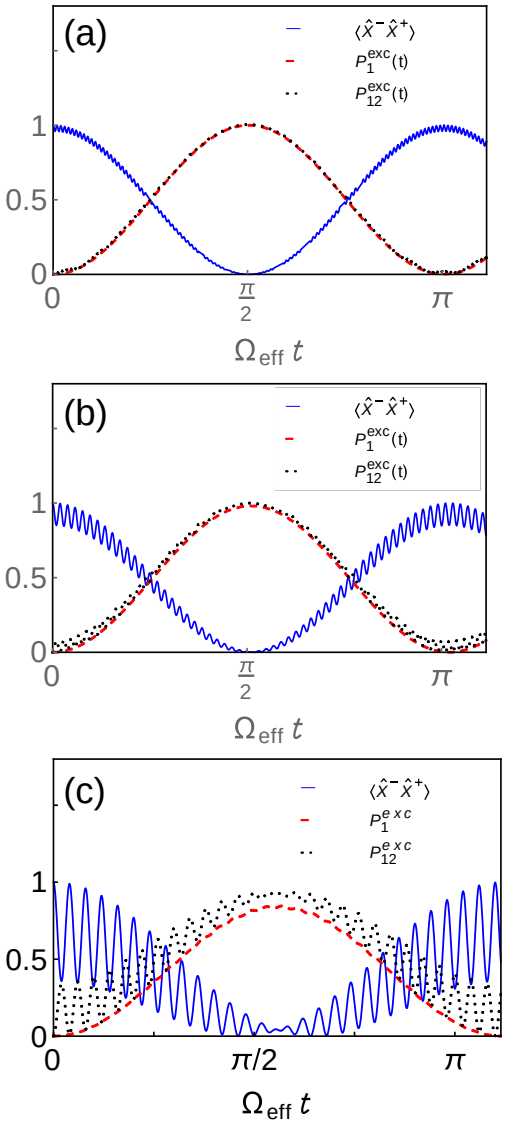

FIG. S5. (Color online) Time evolution of the mean intracavity photon number $\langle \hat{X}^- \hat{X}^+ \rangle$, of the probability that atom 1 is in one of the two excited states $P_1^{\rm exc}(t)$, and the probability that both atoms are excited $P_{12}^{\rm exc}(t)$, calculatd for different normalized detunings (from the upper to the lower panels, $\Delta/\omega_{eg} = 1,\, 0.5,\, 0.2$).

Starting from the initial state $|g,g,1\rangle$, Fig. S5 describes the time evolution of the mean

intracavity photon number $\langle \hat{X}^- \hat{X}^+ \rangle$, of the probability that atom 1 (equal to that of atom 2, being the two atoms identical) is in one of the two excited states $P_1^{\rm exc}(t)$, and the probability that both atoms are excited $P_{12}^{\rm exc}(t)$. Calculations have been carried out for different normalized detunings (from the upper to the lower panels, $\Delta/\omega_{eg} = 1,\, 0.5,\, 0.2$). We also used $\Omega_{\rm eff} = 5 \times 10^{-3}\omega_{eg}$, $\lambda' = 0.1$. Damping has not been included. Figure S5 shows that, when the detuning Δ is large as compared to the coupling strength λ', the influence of the additional transition is negligible. When Δ approaches λ', fast oscillations, due to the partial occupation of state $|f\rangle$ appears and a lowering of the two-atom correlation can be observed.

IV. NONIDENTICAL QUBITS

We have also considered the case of nonidentical qubits. The system Hamiltonian is,

$$\hat{H}_0 = \hat{H}_{\rm q} + \hat{H}_{\rm c} + \hat{X} \sum_{i=1}^{2} \lambda (\cos\theta\, \hat{\sigma}_x^{(i)} + \sin\theta\, \hat{\sigma}_z^{(i)}) \,, \tag{9}$$

where $\hat{H}_{\rm q} = \sum_{i=1}^{2} \omega_{{\rm q}i}/2\hat{\sigma}_z^{(i)}$. It is useful to define $\omega_0 = (\omega_{\rm q1} + \omega_{\rm q2})/2$.

Figure S6a displays the lowest energy states (we report the frequency differences $\omega_{i,0} = \omega_i - \omega_0$) as a function of the resonator frequency resulting from the numerical diagonalization of the total Hamiltonian in Eq. (9). We used $\omega_{\rm q1} = 1.2\,\omega_0$, $\omega_{\rm q2} = 0.8\,\omega_0$, $\lambda_1/\omega_0 = 0.12\,\omega_0$, $\lambda_2/\omega_0 = 0.8$ and $\theta = \pi/6$. At $\omega_{\rm c} \simeq 1.974\,\omega_{\rm c}$ an apparent crossing can be observed. Actually, what appears as a crossing on this scale, it turns out to be a splitting anticrossing on an enlarged view as in Fig. S6b.

Figure S7 displays the numerically-calculated dynamics of the photon number $\langle \hat{X}^- \hat{X}^+ \rangle$, of the mean excitation number $\langle \hat{C}_i^- \hat{C}_i^+ \rangle$ for qubit1 1 and 2, and of the two-qubit correlation $G_{\rm q}^{(2)} \equiv \langle \hat{C}_1^- \hat{C}_2^- \hat{C}_2^+ \hat{C}_1^+ \rangle$. Vacuum Rabi oscillations showing the reversible excitation exchange between the qubits and the resonator are clearly visible. We find that also for nonidentical qubits, it results $\langle \hat{C}_1^- \hat{C}_1^+ \rangle \simeq \langle \hat{C}_2^- \hat{C}_2^+ \rangle \simeq G_{\rm q}^{(2)}$. This result *further confirms the simultaneous and joint nature of this multiatom process.*

V. HIGHER LIGHT-MATTER COUPLING STRENGTH

Here we present results for a qubit-cavity coupling strength higher than that consider in the main paper. Specifically, we consider a normlized coupling strength $\lambda = 0.2\,\omega_{\rm q}$. The

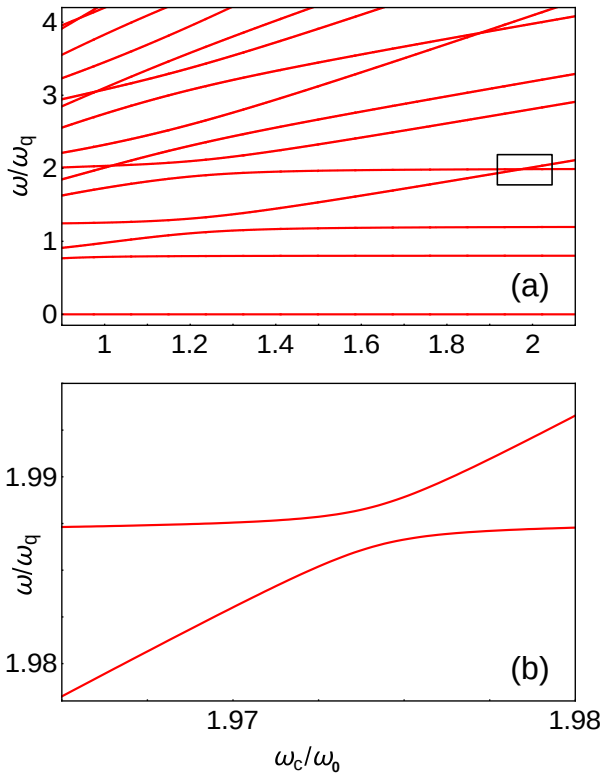

FIG. S6. (Color online) Energy levels as a function of ω_c/ω_0 for two non identical qubits qubits interacting with a resonator. (a) Frequency differences $\omega_{i,0} = \omega_i - \omega_0$ for the lowest energy eigenstates of Hamiltonian (9) as a function of ω_c/ω_0. (b) Enlarged view of the spectral region delimited by a square in panel (a). This shows an avoided-level crossing, demonstrating the coupling between the states $|g, g, 1\rangle$ and $|e, e, 0\rangle$ in the case of noidentical qubits.

other parameters are the same used for the calculation presented in Fig. 2 of the paper. Figure S8 displays the energy levels and a splittting, significantly larger than that shown Fig. 2b in the paper, can be observed in Fig. S8b.

Figure S9 displays the numerically-calculated dynamics of the photon number $\langle \hat{X}^- \hat{X}^+ \rangle$, of the mean excitation number $\langle \hat{C}_1^- \hat{C}_1^+ \rangle$ for qubit 1 (which, of course, coincides with that of qubit 2), and of the two-qubit correlation $G_q^{(2)} \equiv \langle \hat{C}_1^- \hat{C}_2^- \hat{C}_2^+ \hat{C}_1^+ \rangle$. Vacuum Rabi oscillations showing the reversible excitation exchange between the qubits and the resonator are clearly visible. The main effect of increasing the coupling strength, besides the obvious decrease of the effectiv Rabi period, is the increasing of the minimum value of $\langle \hat{X}^- \hat{X}^+ \rangle$ when $\langle \hat{C}_1^- \hat{C}_1^+ \rangle$ is maximum. This nonzero minimum occurs because the two-qubit excited state, owing to the

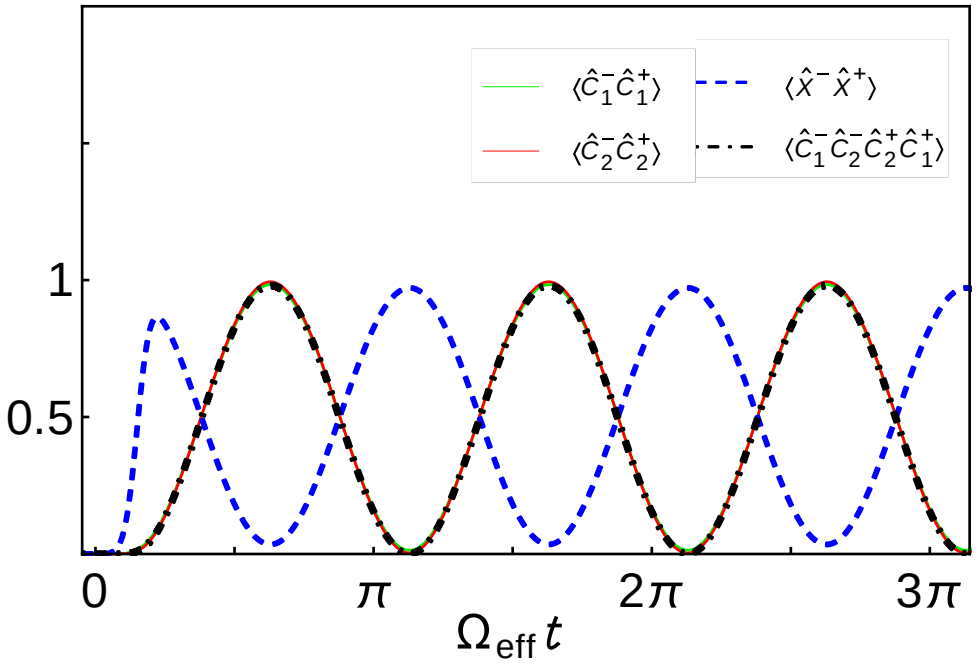

FIG. S7. (Color online) Time evolution of the cavity mean photon number $\langle \hat{X}^- \hat{X}^+ \rangle$ (dotted blue curve), qubit 1 mean excitation number $\langle \hat{C}_1^- \hat{C}_1^+ \rangle$ (continuous black curve), and the zero-delay three-qubit correlation function $G_{\mathrm{q}}^{(3)} = \langle \hat{C}_1^- \hat{C}_2^- \hat{C}_3^- \hat{C}_3^+ \hat{C}_2^+ \hat{C}_1^+ \rangle$ (dashed red curve) after the arrival of a π-like Gaussian pulse initially exciting the resonator. After the arrival of the pulse, the system undergoes vacuum Rabi oscillations showing the reversible joint absorption and re-emission of one photon by three qubits. $\langle \hat{C}_1^- \hat{C}_1^+ \rangle$ and $G_{\mathrm{q}}^{(3)}(t)$ are almost coincident.

same processes inducing its coupling with the one-photon state, acquires a dipole transition matrix element, so that this state is able to emit photons decaying to the lower energy states. The increase of its value in the present case is due to the increase of this transition matrix when the coupling strength λ increases.

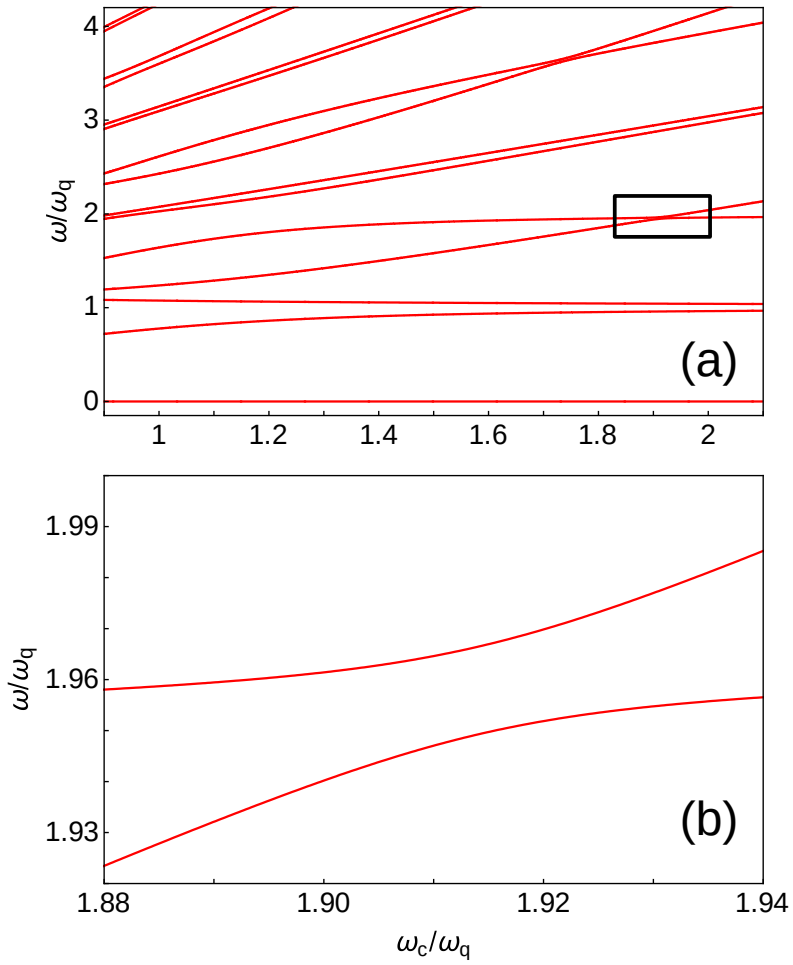

FIG. S8. (Color online) Higher light-matter coupling strength. (a) Frequency differences $\omega_{i,0} = \omega_i - \omega_0$ for the lowest energy eigenstates of Hamiltonian (9) as a function of ω_c/ω_q, obtained for an higher coupling strength $\lambda/\omega_q = 0.2$. (b) Enlarged view of the spectral region delimited by a square in panel (a). This shows an avoided-level crossing, demonstrating the coupling between the states $|g, g, 1\rangle$ and $|e, e, 0\rangle$ in the case of noidentical qubits.

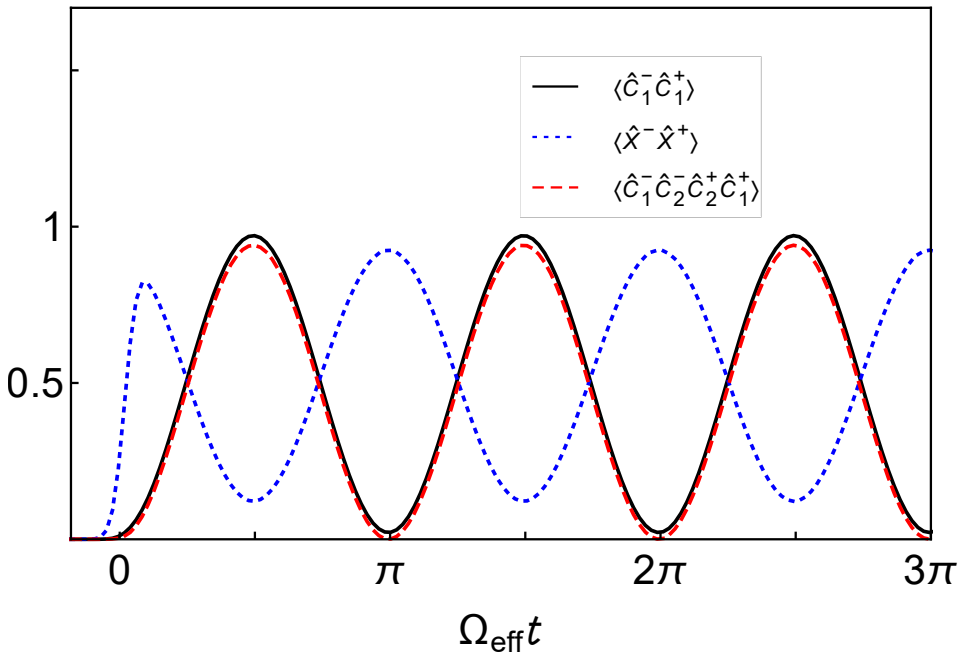

FIG. S9. (Color online) Higher light-matter coupling strength: time evolution of the cavity mean photon number $\langle \hat{X}^- \hat{X}^+ \rangle$ (dotted blue curve), qubit 1 mean excitation number $\langle \hat{C}_1^- \hat{C}_1^+ \rangle$ (continuous black curve), and the zero-delay two-qubit correlation function $G_{\text{q}}^{(2)} = \langle \hat{C}_1^- \hat{C}_2^- \hat{C}_2^+ \hat{C}_1^+ \rangle$ (dashed red curve) after the arrival of a π-like Gaussian pulse initially exciting the resonator. After the arrival of the pulse, the system undergoes vacuum Rabi oscillations showing the reversible joint absorption and re-emission of one photon by three qubits.